Journal of Engineering Physics and Thermophysics, Vol. 66, No. 6, 1994

MATHEMATICAL MODELING OF THE AERODYNAMICS AND PHYSICOCHEMICAL PROCESSES IN THE FREEBOARD ZONE OF A CIRCULATING FLUIDIZED BED FURNACE. 3. BOUNDARY CONDITIONS. SOME NUMERICAL RESULTS

B. B. Rokhman and A. A. Shraiber

UDC 532.529:662.62:66.096.3

Boundary conditions are formulated for differential equations describing two-dimensional motion of gas and polydisperse coke and ash particles in a high-concentration flow [1, 2]. Specific features of the aerodynamics of the pneumatic transport zone in the freeboard zone was investigated numerically in a circulating fluidized bed reactor. The model constructed is verified by experimental data [3].

In Parts 1 [1] and 2 [2] of the present work a closed system of equations was obtained for axisymmetric motion of gas and polydisperse coke and ash particles in the pneumatic transport zone (PTZ) of the freeboard zone in a circulating fluidized bed reactor. This system includes equations of transfer of mass (1) and (2), momentum (3)–(5), and kinetic energy of fluctuation motion (7) and (11) of the components (see [1]). Boundary conditions for these equations should be prescribed on the flow axis, on the reactor wall, and in the entrance section. From symmetry considerations on the axis we have

$$\overline{v}_{\mathrm{ga}} = \overline{v}_{i\mathrm{a}} = 0\,; \quad \left(\frac{\partial \overline{u}_{\mathrm{g}}}{\partial r}\right)_{\mathrm{a}} = \left(\frac{\partial \overline{u}_i}{\partial r}\right)_{\mathrm{a}} = \left(\frac{\partial \overline{\beta}_i}{\partial r}\right)_{\mathrm{a}} = \left(\frac{\partial k_{\mathrm{g}}}{\partial r}\right)_{\mathrm{a}} = \left(\frac{\partial k_i}{\partial r}\right)_{\mathrm{a}} = 0\,. \tag{1}$$

It is evident that on the wall

$$\overline{u}_{\mathrm{gw}} = k_{\mathrm{gw}} = \overline{v}_{i\mathrm{w}} = 0\,. \tag{2}$$

Since the wall is assumed to be impermeable to the particles, use will be made of the vanishing of the total (convective and diffusion) flow in the radial direction, so that

$$(\partial \overline{\beta}_i / \partial r)_{\mathrm{w}} = 0\,. \tag{3}$$

In [4], to derive the boundary condition on the wall for the equation of the axial motion of the particles, two flows of particles in the peripheral zone (to and from the wall) are brought into consideration. The velocities of the flows are $\overline{u}_{i1}$, $\overline{v}_{i1}$ and $\overline{u}_{i2}$, $\overline{v}_{i2}$, respectively. These quantities are related by the equation of a single collision (1) from [2], from which it follows that

$$\overline{u}_{i2} = \overline{u}_{i1}\,(5 + 2k_\tau)/7\,; \quad \overline{v}_{i2} = k_n \overline{v}_{i1}\,. \tag{4}$$

Since the flows considered should be equal to each other, the concentrations in them are inversely proportional to the absolute values of the radial velocities, so that the average velocity near the wall is

$$\overline{u}_{i\mathrm{w}} = (\overline{u}_{i2} - k_n \overline{u}_{i1})/(1 - k_n)\,. \tag{5}$$

Institute of Problems of Energy Conservation, Academy of Sciences of Ukraine, Kiev, Ukraine. Translated from Inzhenerno-Fizicheskii Zhurnal, Vol. 66, No. 6, pp. 681-688, June, 1994. Original article submitted April 22, 1992.

1062-0125/94/6606-0607$12.50

Next, similarly to (5), the quantities

$$[\overline{(\varphi_2 - \varphi_w)(\psi_2 - \psi_w)} - k_n \overline{(\varphi_1 - \varphi_w)(\psi_1 - \psi_w)}]/(1 - k_n), \quad (\varphi, \psi = \bar{u}_i, \bar{v}_i),$$

are calculated. They are identified incorrectly with the correlations of the fluctuation components $\overline{(\varphi'\psi')}_w$. As a result, in [4], using the analog of Boussinesq hypothesis (8) from [1], the following boundary condition is obtained:

$$(\partial \bar{u}_i/\partial r)_w = f_1 \bar{u}_{iw} (\overline{v_i'^2})_w/\nu_i, \quad f_1 = f(k_n, k_\tau),$$

Naturally, it cannot be recognized as justified. A more rigorous approach involves concepts of the dynamics of rarefied gases. Assuming that over the length L (see Eq. (8) in [2]) the particle velocity changes but slightly and expanding the function $\bar{u}_i(r)$ in a series, it is found that particles approaching the wall have the velocity

$$\bar{u}_{i1} = \bar{u}_{iw} - 0.5L (\partial \bar{u}_i/\partial r)_w \tag{6}$$

(it is taken into consideration here that the average projection of L on the r axis is $L/2$ [2]). From Eqs. (4)–(6) and expression (8) from [2], after simple manipulations, we have

$$\bar{u}_{iw} = \frac{\langle \delta \rangle}{24\sqrt{2}\,\bar{\beta}_e (1 - k_\tau)} \left(\frac{\partial \bar{u}_i}{\partial r}\right)_w (7k_n - 2k_\tau - 5) \tag{7}$$

($\langle\delta\rangle$ is the average particle size, β_e is the equivalent particle concentration from [2], for a monodisperse material $\langle\delta\rangle = \delta$, $\bar{\beta}_e = \bar{\beta}_p$). At $k_\tau = 1$ (smooth surfaces) Eq. (7) should be replaced by $(\partial \bar{u}_i/\partial r)_w = 0$.

The boundary condition for k_i can be obtained in a way similar to that used for (7). It should be taken into consideration that according to (4), after collision the "normal" component of k_i becomes equal to $k_i k_n^2/3$ and the "tangential" component, to $2k_i(5 + 2k_\tau)^2/147$ (the fluctuations are assumed to be spherically symmetric [2]). As a result,

$$k_{iw} \frac{3k_n - f_2}{3 - f_2} \frac{L}{2} \left(\frac{\partial k_i}{\partial r}\right)_w; \quad f_2 \equiv k_n^2 + \frac{2}{49}(5 + 2k_\tau)^2. \tag{8}$$

The values of the unknown functions in the entrance section of the PTZ ($z = 0$) are determined from the solution of the problem of the motion of the flow in the transition zone. However, this problem will be considered later; therefore, here use will be made of the hypothesis of the uniformity of the flow at $z = 0$.

The complete system of aerodynamic equations in the PTZ contains three types of equations. Equations (2), (3), (7), and (11) from [1] are parabolic (in view of the fact that the correlations of the fluctuation parameters are approximated as was done in (8) from [1], and a difference analog of the six-point pattern suggested in [5] is used here. Hyperbolic equations (4) and (5) from [1] are approximated following an implicit scheme of the first order [6], and discontinuity equation (1) from [1], following an explicit four-point scheme (see also [7]). In the following, a number of examples of numerical results are presented.

Figure 1 presents numerical values of the averaged longitudinal velocities of gas (solid lines) and monodisperse particles $\delta = 500$ μm (dot-dash lines) in the channel $R = 15$ mm in comparison with experimental data [3]. Curve 1 in Fig. 1a is calculated by the present method and curve 2 is calculated neglecting pseudoturbulent motion of the particles [2] and without using transfer equation (11) from [1] (i.e., the parameters of particle fluctuations were determined in a locally homogeneous approximation similarly to [7]). It is evident that inclusion of pseudoturbulence gives a better description of the experimental data. In Fig. 1c points and curves 3 correspond to $\kappa = 3.6$; a certain divergence from the experimnetal data is seen here. It is also noticeable that curve 3 does not reflect an important qualitative regularity, namely, the presence of a maximum on the curve $\bar{u}_p(r)$. However, this is not indicative of serious drawbacks of the model: lines 4 show results of similar calculations at $\kappa = 6$ and here the shape of the curve $\bar{u}_p(r)$ is fully consistent with the experiment.

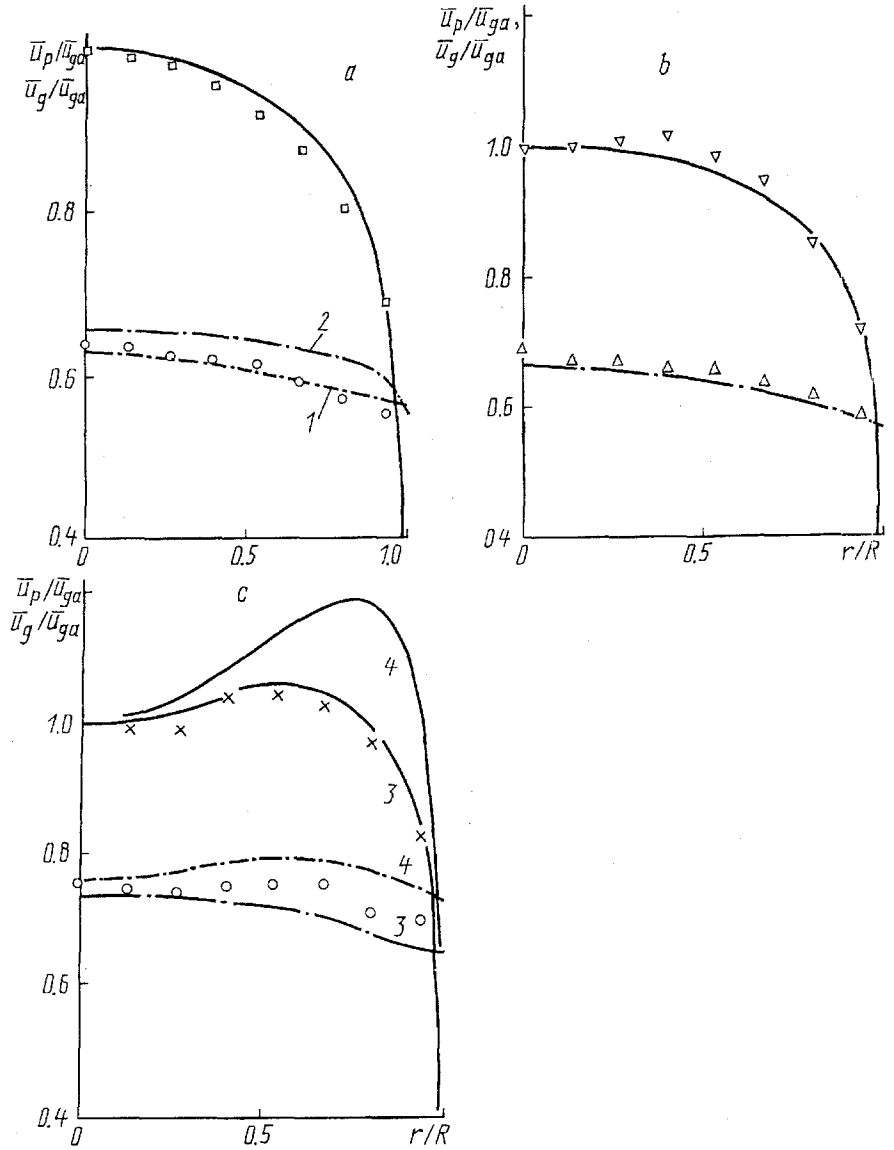

Fig. 1. Cross-sectional distribution of axial velocities of phases in the flow: a) $\kappa = 1.1$; $\bar{u}_{gm} = 7.96$ m/sec; b) $\kappa = 2$, $\bar{u}_{gm} = 8$ m/sec; c) $\kappa = 3.6$ and 6, $\bar{u}_{gm} = 7.89$ m/sec.

Figures 2–6 illustrate distinct features of the aerodynamics of a coke-ash flow in the stabilized area of a PTZ. The radius of the channel is assumed to be $R = 100$ mm (a typical scale of laboratory setups), the average velocity of gas is $\bar{u}_{gm} = 6$ m/sec, and the total concentration of particles is $\kappa = 6$. Three cases were considered: A is a monodisperse flow with ash particles $\delta_l = 300$ μm; B is motion of ash particles $\delta_l = 300$ μm and a coke fraction ($\delta_j = 150-300$ μm); C is a flow with two fractions of ash ($\delta_1 = 300$ μm and $\delta_2 = 180$ μm) and coke ($\delta_1 = 250$ μm and $\delta_2 = 150$ μm). The concentration of coke particles was assumed to be 0.3κ.

In Fig. 2, which shows data for case A, it is clearly seen that the changes in k_g (except for the peripheral zone, $k_{gw} = 0$) and k_p are opposite to the change in the true concentration of the particles. A maximum at $r \sim 0.92$ R on the curve $k_g(r)$ can probably be explained by the effect of dissipation of the turbulent energy due to fluctuation slip (see Eq. (11) from [1] and Eq. (21) from [2]). The behavior of the curve $k_p(r)$ can be ascribed to the fact that in accordance with the pseudoturbulence model adopted for a monodisperse material [2], the rate of generation of fluctuation energy is independent of $\bar{\beta}_p$, while the rate of energy dissipation is proportional to $\bar{\beta}_p^2$ (see Eq. (11) from [1] and Eqs. (13) and (14) from [2]). One more argument will be given to explain the relation between k_p and $\bar{\beta}_p$. Integration of continuity equation (2) from [1] for a stabilized area

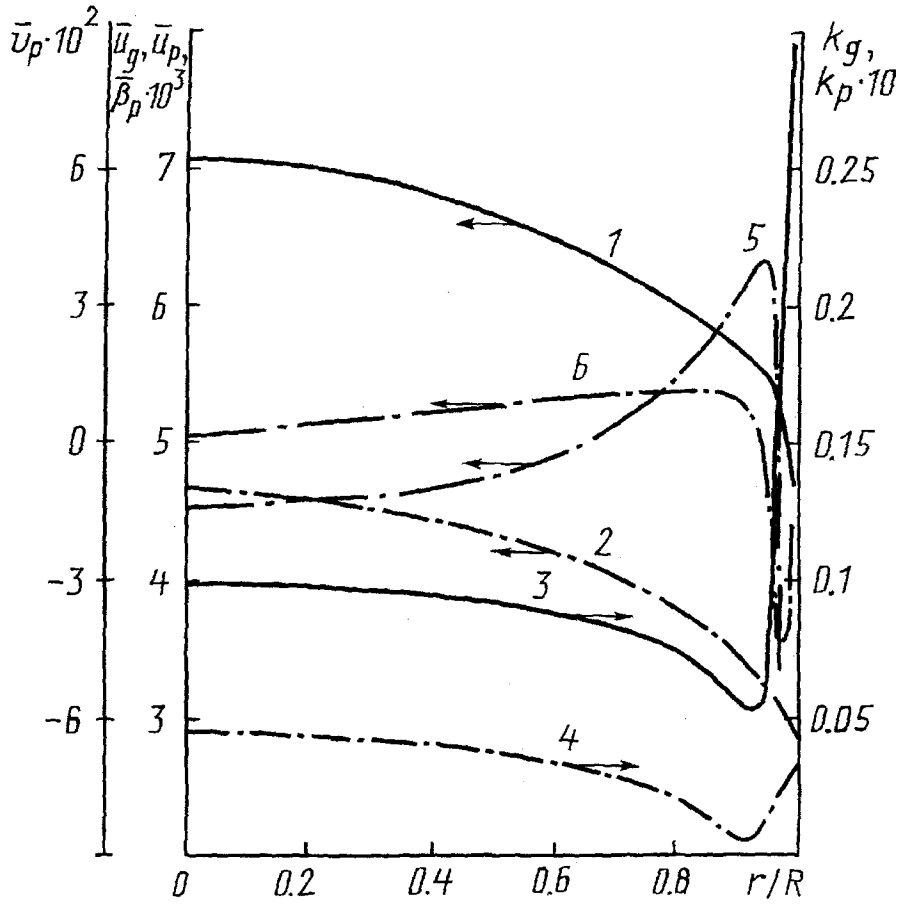

Fig. 2. Cross-sectional distribution of axial velocities of gas (1) and particles (2), kinetic energies of fluctuation motion of the gas (3) and particles (4), and concentration and radial velocity (6) of ash in the flow. v_p, m/sec; k_g, k_p, m^2/sec^2; $\bar{u}_g$, $\bar{u}_p$, m/sec.

$$\frac{1}{r}\frac{\partial}{\partial r}\left[r\left(\bar{\beta}_p \bar{v}_p - D_p \frac{\partial \bar{\beta}_p}{\partial r}\right)\right] = 0$$

with boundary conditions (2) and (3) gives

$$\bar{\beta}_p \bar{v}_p - D_p \partial \bar{\beta}_p / \partial r = 0 . \tag{9}$$

Neglecting the drag force and the correlation $\overline{\beta'_p v'_p}$ compared to $\overline{v'^2_p}$ in Eq. (5) from [1], with account for Eq. (9) we obtain

$$-\partial (r\bar{\beta}_p k_p)/\partial p + \bar{\beta}_p k_p = 0 ,$$

i.e., $\bar{\beta}_p k_p = C$ (C is the integration constant), which is in good agreement with the behavior of curves 4 and 5 (Fig. 2). Assuming $D_p = \nu_p$ and using expressions (8) and (22) from [2], instead of (9) we can write

$$\partial \bar{\beta}_p / \partial r = (\bar{\beta}_p)^{5/2} \bar{v}_p / C_1 ; \quad C_1 \equiv \sqrt{C}\,\delta/18 ,$$

or upon integration,

$$\bar{\beta}_p = \left[(\bar{\beta}_{pa})^{-2/3} - 1.5 C_1^{-1} \int_0^r \bar{v}_p dr\right]^{-2/3} . \tag{10}$$

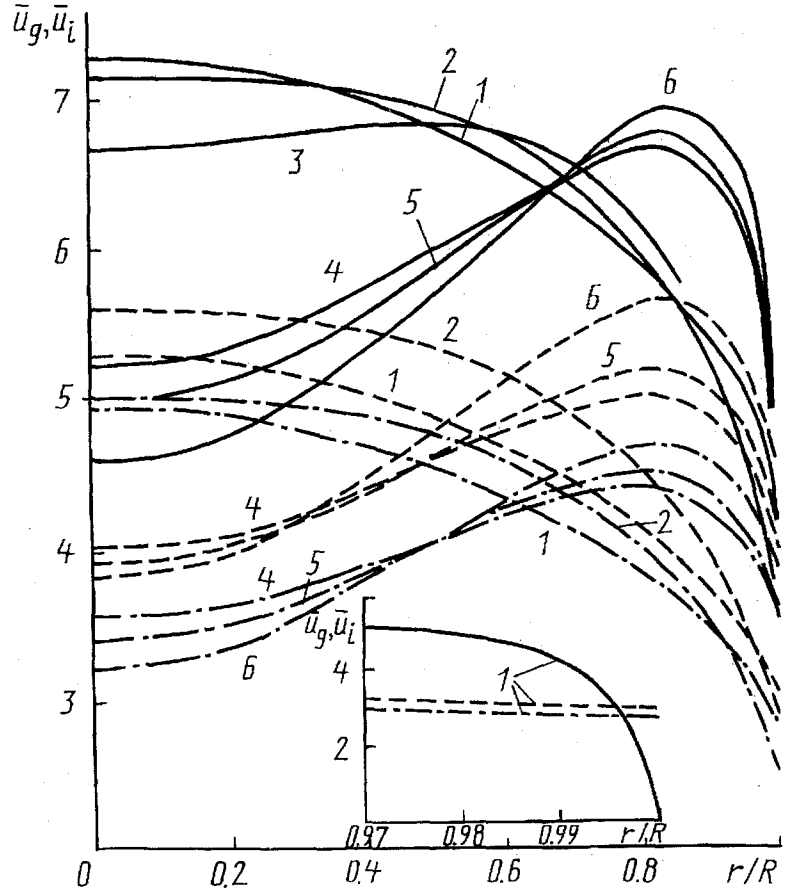

Fig. 3. Axial velocities of gas (solid lines) and particles of coke δ_j (dashed lines) and ash δ_i (dot-dash lines): 1) $\delta_j = 300$ μm; 2) 225; 3) 223.5; 4) 220; 6) 150 μm. $\bar{u}_i$, m/sec.

Formula (10) can easily explain the relation between the functions $\bar{v}_p(r)$ and $\bar{\beta}_p(r)$: in the region of $r < 0.92R$, where the values of $\bar{v}_p$ are positive, the concentration of particles increases, while on the periphery, where the radial velocity is directed toward the axis, it decreases.

Figure 3 shows the distribution of longitudinal velocities of the phases for case *B*. Here one can see two typical shapes of the relations $\bar{u}_g(r)$: with a maximum on the flow axis (curves 1 and 2) or on the periphery. It is interesting that the velocity profile is restructured basically in a very narrow range of the size of the coke particles (cf. curves 2, 3, and 4). To explain these results, the equation of longitudinal motion of gas (3) from [1] for the axial region (where $\partial \bar{u}_g / \partial r = 0$) will be written, neglecting small terms, as

$$\bar{\rho}_g \nu_t \frac{\partial^2 \bar{u}_g}{\partial r^2} \approx \sum_i \bar{F}_{iz} + \frac{\partial \bar{p}}{\partial z}, \tag{11}$$

where Σ means the sum over all fractions of the particles. Since $\partial \bar{p} / \partial z$ is always less than zero, in the case where the total drag force is larger than the absolute value of the pressure gradient, the derivative $\partial^2 \bar{u}_g / \partial r^2 > 0$, and the function $\bar{u}_g(r)$ has a minimum on the flow axis. In opposite situations a maximum is observed at the point $r = 0$. Calculations have shown that $\partial \bar{p} / \partial z$ depends but slightly on the size of the coke particles. Meanwhile, the drag force changes quite substantially and its value depends primarily on the three parameters $\bar{u}_g - \bar{u}_j$, $\bar{\beta}_j$, and δ_j^2. For example, compare curves 2 and 6 in Fig. 3. In the former case, the slip velocity is 1.5–2 times larger (depending on the particle "species"). This change does not compensate, however, for a decrease in the total concentration of particles (Fig. 4) and in δ_j^2, so that ultimately, the drag force turns out to be much smaller at $\delta_j = 225$ μm. It is

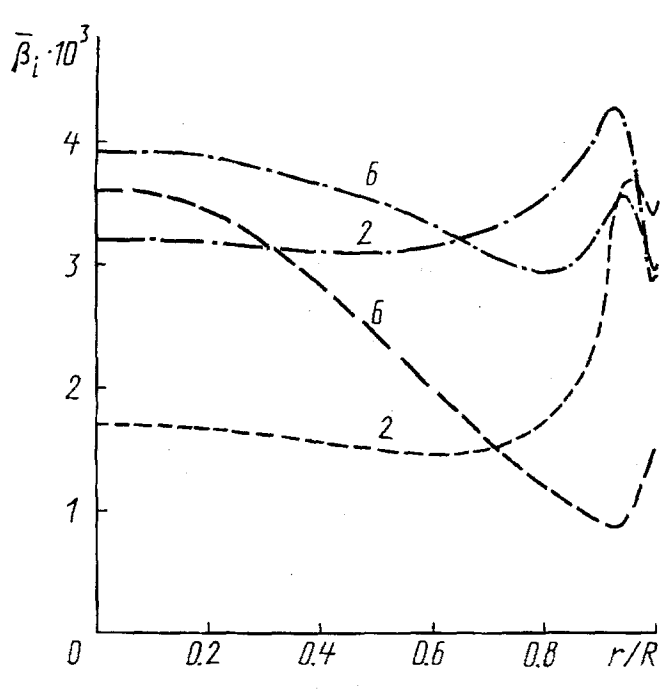

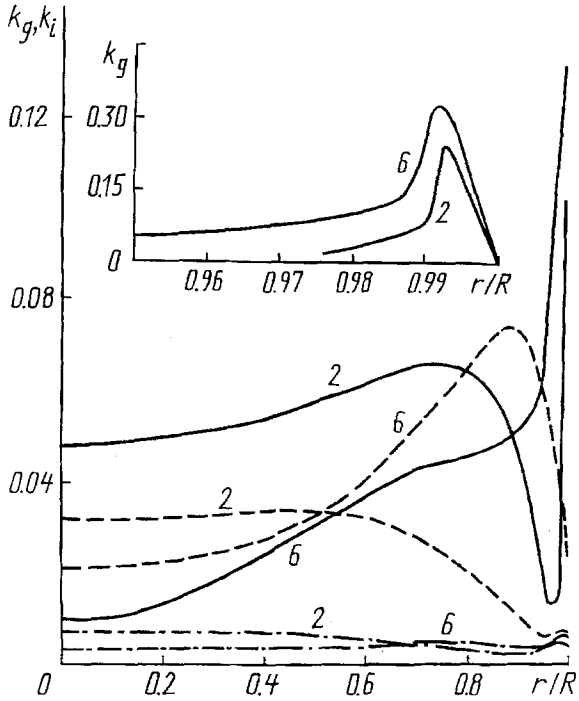

Fig. 4. Concentration profile of the disperse phase for case *B* (the same notation as in Fig. 3).

Fig. 5. Kinetic energy of fluctuation motion of gas and particles for case *B* (the same notation as in Fig. 3).

likely that depending on the relation between $\Sigma \bar{F}_{iz}$ and $\partial \bar{p}/\partial z$, the system tends to one of two stable states (curves 1 and 2 or 4–6 in Fig. 3).

Comparison of Figs. 3 and 4 shows that the distributions of the concentration of particles and the velocity of gas are generally opposite, i.e., in the zone of higher concentrations the inverse effect of the particles on the gas results in a decrease in the axial velocity of the gas. In particular, in case 6 ($\delta_j = 150$ μm) a decrease in $\bar{\beta}_i$ in the range of $r = (0-0.85)R$ corresponds to an increase in $\bar{u}_g$, while in case 2 ($\delta_j = 225$ μm), the region of $r \lesssim 0.4R$ is characterized by almost constant values of both parameters. The zone near the wall, where boundary condition (2) has a substantial effect on the distribution of the velocity of the gas, is the only exception. The curves $\bar{u}_i(r)$ in Fig. 3 are generally similar to the curves $\bar{u}_g(r)$ and the slip value is lower, the smaller δ_j. For coke particles this can be explained by a change in the drag force, and for ash particles (remember that $\delta_l = 300$ for all cases), by interaction between the fractions (see Eq. (4) in [1]). Near the wall, where the velocity of the gas decreases sharply, the particles appear ahead of the gas; here the drag force becomes negative and suspension of the particles is caused mainly by the action of the Reynolds stresses.

In Fig. 5 it is seen that while moving in the flow, fine, light particles are involved in more intense random motion. This can be explained primarily by the fact that the rate of generation of the energy of fluctuation motion of particles i is proportional to m_k^2 in the interaction of fractions $k-i$ (see Eqs. (1), (5), and (6) in [2]). Moreover, the interfractional slip velocity, which is larger for case 6, also has a certain effect on the value of k_i (see Fig. 3). It is interesting that as in the case of a monodisperse material (see Fig. 2), the general behavior of the curves $k_i(r)$ is opposite to that of the curves $\bar{\beta}_i(r)$, i.e., the arguments given above on the relation between k and $\bar{p}$ are also valid to a certain extent for a polydisperse composition of the particles.

In Fig. 6a it is clearly seen that the velocities of the fractions stratify in accordance with the size and density of the particles. Interaction of the fractions results in substantial leveling of the concentration profiles (Fig. 6b). It should be noted that there is one more important distinctive feature in this case: in a substantial part of the cross section ($r \lesssim 0.97R$), the fluctuation energy of fine coke particles exceeds the energy of gas fluctuations by several

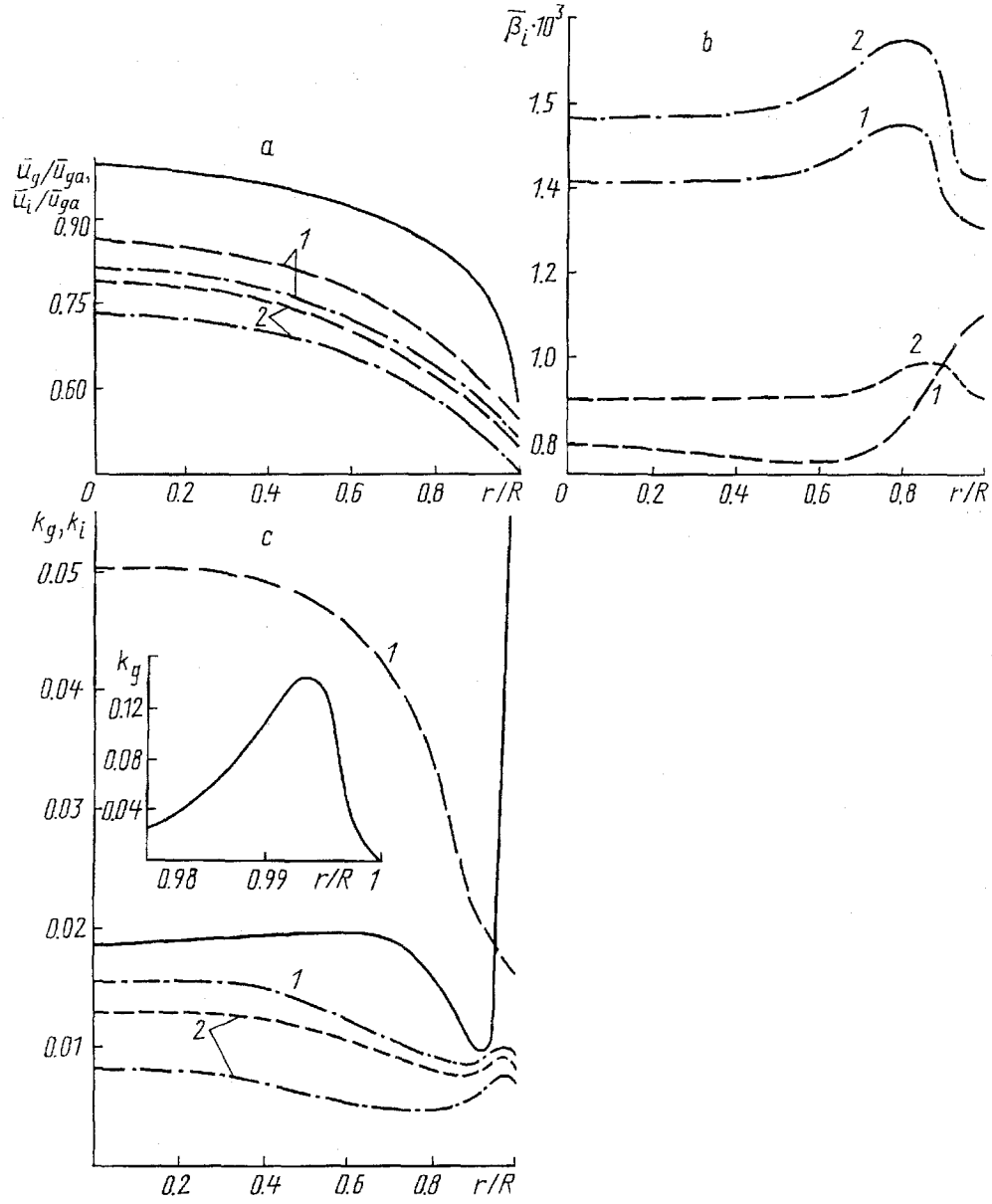

Fig. 6. Parameters of a two-phase polydisperse flow for case C: a) axial velocities of phases; b) concentration of particles; c) energy of fluctuation motion; 1) fine particles; 2) large particles (the remaining notation is the same as in Fig. 3). k_i, m^2/sec^2.

times (cf. Figs. 2 and 5). This indicates that pseudoturbulent transfer prevails in the aerodynamics of high-concentration polydisperse flows.

NOTATION

z, r, longitudinal and radial coordinates; u, v, projections of the velocity vector onto the z, r, axes; k, kinetic energy of the fluctuation motion; β, true volume concentration; k_n, k_τ, reduction coefficients of the normal and tangential velocity components in collision ($k_n \leq 0$); ν, D, viscosity and diffusion coefficients; L, mean free path of a particle between successive collisions; δ, particle size; R, radius of the channel; κ, mass flow rate; p, pressure; F, drag force; m, particle mass. Subscripts and superscripts: g, p, gas, particles; 1, 2, ... , i, j, l, fraction number (for a polydisperse matrial the subscript p is omitted); a, flow axis; w, wall, m, mean over the cross section; t, turbulent analog; $\bar{}$, $'$, averaged and fluctuation components.

REFERENCES

1. B. B. Rokhman and A. A. Shraiber, Inzh.-Fiz. Zh., **65**, No. 5, 521-526 (1993).
2. B. B. Rokhman and A. A. Shraiber, Inzh.-Fiz. Zh., **66**, No. 2, 159-167 (1994).
3. Y. Tsyji, Y. Morikawa, and H. Shiomi, J. Fluid Mech., **139**, 417-434 (1984).
4. L. V. Kondrat'ev, A Model and a Numerical Investigation of a Turbulent Flow of a Suspension in a Tube [in Russian], Candidate's Thesis, Leningrad (1989).
5. I. Yu. Borislavskaya and L. A. Chudov, Computation Methods and Programming [in Russian], Moscow (1962), Pt. 1, pp. 167-182.
6. L. A. Dorfman, Numerical Methods in the Gasdynamics of Turbomachines [in Russian], Leningrad (1974).
7. A. A. Shraiber, L. B. Gavin, V. A. Naumov, and V. P. Yatsenko, Turbulent Flows of a Gas Suspension [in Russian], Kiev (1987).